Experimental investigation and characterization of micro resistance welding with an electro-thermal actuator

2009 J. Micromech. Microeng. 19 025001

(http://iopscience.iop.org/0960-1317/19/2/025001)

J. Micromech. Microeng. **19** (2009) 025001 (8pp) doi:10.1088/0960-1317/19/2/025001

Experimental investigation and characterization of micro resistance welding with an electro-thermal actuator

Chun-Wei Chang, Cheng-Chi Yeh and Wensyang Hsu[1]

Department of Mechanical Engineering, National Chiao Tung University, 1001 Ta Hsueh Road, Hsinchu 30010, Taiwan, Republic of China

E-mail: whsu@mail.nctu.edu.tw

Received 8 June 2008, in final form 13 November 2008
Published 14 January 2009
Online at stacks.iop.org/JMM/19/025001

Abstract

Resistance welding is a common scheme of assembly on the macro scale by pressing together two workpieces with current passing through them to generate joule heating at the contact region due to high contact resistance. However, micro assembly by resistance welding is seldom reported. Here, resistance welding with an electro-thermal microactuator to assemble micro Ni structures is experimentally investigated and characterized. The bent-beam electro-thermal microactuator is designed to provide the necessary displacements and pressing forces. The two-mask metal-based surface micromachining process is adopted to fabricate the micro Ni structures. The calibrated initial contact resistance is shown to decrease with increasing contact pressure. Furthermore, stronger welding strength is achieved at a smaller initial contact resistance, which indicates that a larger clamping force would enhance the welding strength as large as 3.09 MPa (74.4 μN) at a contact resistance of 2.7 Ω here. The input welding energy is also found to be a critical factor. In our tests, when welding energy is below the threshold limit of 0.05 J, the welding trials all fail. For the energy between 0.05 J and 1 J, there is a transition from a lower yield of 33.3% to a higher yield of 58.3%. At high welding energy, between 1 and 10 J, 100% yield is achieved. With the demonstration and characterization of micro resistance welding by the electro-thermal microactuator, the scheme proposed here would be helpful in the automation of micro assembly.

1. Introduction

Technologies based on thermal energy have been widely used for bonding, such as fusion bonding [1, 2] and localized heating techniques [3, 4]. With the rapid development of micro electro-mechanical systems (MEMS), thermal fusion has also been a common method to assemble micro structures, either in the vertical or horizontal direction. For example, in the surface tension techniques [5–7], the surface tension is induced by the phase change of low-melting-point material deposited at the hinge to act as an *in situ* driving source, then the micro structures can be moved and assembled at the desired position.

Welding is also a thermal assembly process, which has been extensively used on the macro scale by melting a certain amount of materials between two workpieces. Among different welding technologies, resistance welding is a solder-free approach, which does not need any additional material between the two workpieces. The principle of resistance welding is based on joule heating at a contact point due to its high contact resistance while pressing two workpieces together with current passing through. However, only a very few investigations on micro resistance welding have been reported to assemble micro structures [8–10], where the assembly of micro polysilicon structures was the first reported investigation on micro resistance welding by manually using a probe tip to keep them in contact during welding [8]. Lately, the possibility of using a microactuator to achieve micro resistance welding was proposed and studied in our preliminary investigations [9, 10].

Here, the *in situ* electro-thermal microactuator is designed and analyzed to perform micro resistance welding. The

[1] Author to whom any correspondence should be addressed.

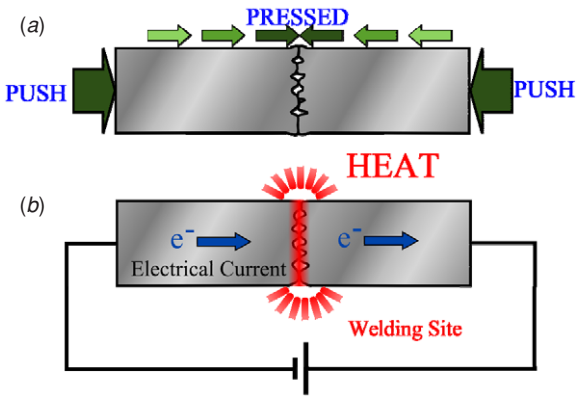

Figure 1. Principle of resistance welding. (*a*) Two workpieces are pushed into contact with each other. (*b*) By applying welding current, material around the contact region can be melted due to local joule heating.

microactuator, which is fabricated next to the micro structures to provide the required pressing force, will be helpful for assembly automation due to its capability of controlling output force electronically. Furthermore, compared to other techniques for raising temperature globally [2], the resistance welding process here only heats a local region, which would be more efficient in energy consumption. To weld a micro nickel structure, the operation parameters, such as contact pressure, contact resistance, welding energy, as well as the joint strength after welding, are experimentally investigated and characterized to identify the feasible operation conditions and welding quality in micro resistance welding.

2. Operation principles

Resistance welding consists of the fusion of materials at contact surfaces by joule heating when the welding current runs through the workpieces. As illustrated in figure 1, after pushing two workpieces together with proper contact pressure, the contact region achieves larger contact resistance. When welding current is applied passing through contact points, the temperature at the contact region is raised due to joule heating.

Resistance welding involves proper coordination of electrical current and mechanical pressure [11]. During resistance welding, electrical current passes from one electrode to another composed by pressed workpieces to generate heat. Sufficient heat has to be generated to raise the temperature of a confined volume to the melting state. During cooling, the two workpieces are still under pressure to ensure adequate mechanical strength. The amount of heat generated can be expressed in terms of voltage, current, and welding time as

$$Q = V I t \tag{1}$$

or in terms of voltage, resistance, and welding time as

$$Q = V^2 t\, R^{-1} \tag{2}$$

where Q represents the heat generated, V the welding voltage, I the welding current, R the resistance at the interface or contact resistance and t the welding time.

In resistance welding, the contact resistance is determined by the conditions of contact points, including pressure and surface properties of contact points, which governs most characteristics of the resistance welding process.

3. Design

3.1. Concept design

The welding structure for this investigation includes three units: an actuation unit (AU), welding unit 1 (WU1) and welding unit 2 (WU2), as shown in figure 2. The actuation unit is composed of an array of bent-beam electro-thermal microactuators [12] which pushes welding unit 1 forward to contact with welding unit 2.

The whole micro resistance welding process can be described in three steps: (1) press, (2) hold and weld and (3) release. The actuation unit, welding unit 1, and welding unit 2 are separate initially. First, the actuation unit pushes welding unit 1 to contact with welding unit 2, as shown in figure 2(*a*). By keeping proper contact pressure, electrical current is applied through the welding site (contact points), as shown in figure 2(*b*). After the proper welding time, the welding current is turned off to cool down. Finally, the clamping force from the actuation unit is released to complete the welding process, as shown in figure 2(*c*).

For bent-beam thermal microactuators, the range of displacement mainly depends on geometry, such as the bent

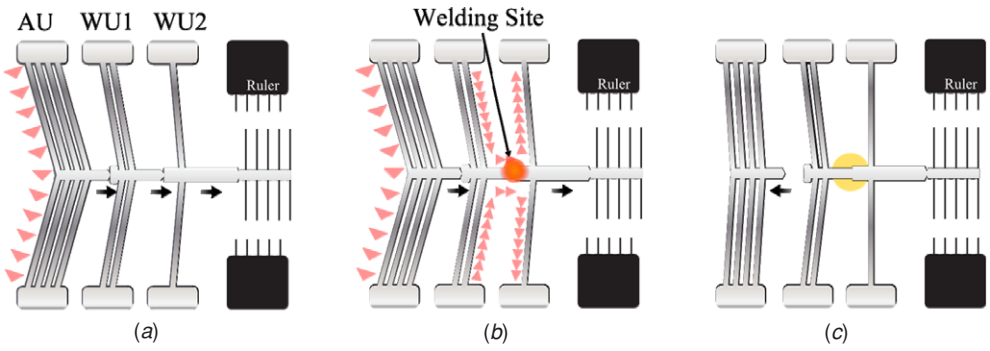

Figure 2. Concept design. (*a*) The actuation unit (AU) pushes welding unit 1 (WU1) to contact with unit 2 (WU2). (*b*) Current passes through the contact point, and then welding current is turned off to cool down under pressure. (*c*) Actuator unit is released.

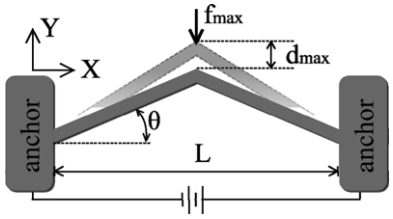

Figure 3. A basic single bent-beam microactuator and the definition of the beam length, L, and the bent angle, θ.

angle and the beam length. In order to ensure sufficient force and displacement, the electro-thermal microactuator needs to be properly designed according to the dimensions of the test structures.

3.2. Bent-beam actuator

The displacement and force of the actuation unit directly affect contact resistance in micro resistance welding. A bent-beam electro-thermal actuator is used here, the design principle of which can be found from previous literature [12, 13]. Since the geometry of the bent-beam electro-thermal microactuator is quite simple, the fabrication process is not complicated. Also, the output force can be easily magnified by increasing the bent-beam number in a parallel way. The performance of bent-beam microactuators could be adjusted easily by the geometry. A single bent-beam microactuator is shown in figure 3, where the maximum displacement of the apex, $d_{\max}$, and maximum output force, $f_{\max}$, can be expressed as [13]

$$d_{\max} = 2\frac{\tan\theta}{k}\tan\frac{kL}{4} - \frac{L}{2}\tan\theta; \qquad k = \sqrt{\frac{F}{EI}} \tag{3}$$

$$f_{\max} = d_{\max} \times K_y; \qquad K_y = \frac{4AE\sin^2\theta}{L} \tag{4}$$

where θ represents the bent angle, L the beam length, F the reaction force along the x-axis at the anchors, E the Young's modulus, I the moment of inertia of the beam and A the cross-sectional area of the beam. The maximum force, $f_{\max}$, is defined as the required force to push the apex back to its original position.

As listed in equation (3), the maximum displacement and maximum force are functions of the beam dimensions, the bent angle and material properties. In general, at a given temperature difference, the larger beam length, L, or the smaller bent angle, θ, would result in larger peak displacement, $d_{\max}$, and smaller peak force, $f_{\max}$ [13]. Connecting these microactuators in parallel can further magnify the maximum force. These equations and design principles provide quick and simple guidelines for the initial concept design of microactuator geometry at the early stage. However, the behavior of the bent-beam microactuator at different temperatures needs to be further analyzed.

3.3. Finite element analysis

Further analysis on the bent-beam microactuator is performed by the finite element method through the software ANSYS. From the finite element analysis (FEA), the beam length

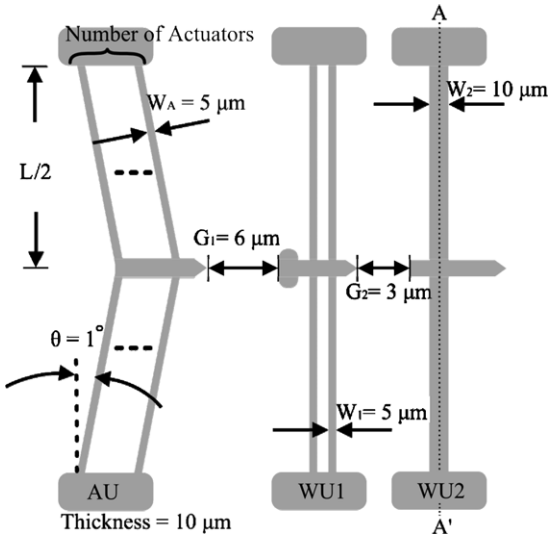

Figure 4. Dimensions of the welding structure.

Table 1. Material properties of nickel adopted in FEA.

Modulus of elasticity (GPa)	207
Density (kg m^{-3})	8880
Coefficient of thermal expansion (10^{-6} K^{-1})	12.7
Poisson ratio	0.31
Thermal conductivity (W m^{-1} K^{-1})	90.5
Specific heat (J kg^{-1} K^{-1})	443
Resistivity (10^{-8} Ω m)	13.5

to provide sufficient displacement can be more precisely determined as short as possible to avoid stiction because a longer beam would reduce the restoring force against the surface tension during releasing. Then, the performance with different numbers of bent beams in the array is simulated to determine the output force for determining the proper number of bent beams in the bent-beam array.

Figure 4 illustrates the dimensions of the proposed test structure design without specifying the number of bent beams and the beam length. The determination of these dimensions mainly depends on our fabrication capability. The gaps, G_1 and G_2, between these units are 6 μm and 3 μm, respectively, which means that the maximum displacement of the actuation unit has to reach at least 9 μm to push welding unit 1 to contact with welding unit 2. Due to the beam stiffness of welding units 1 and 2, these beams also act as mechanical springs, K_1 and K_2, respectively, to resist the actuation force. The material properties of nickel adopted in the FEA are listed in table 1. In simulation, the highest temperature is limited to 400 °C to prevent degeneration of nickel [13].

The performance of bent-beam electro-thermal microactuators resulting from the FEA calculations is given in figure 5. Figure 5(a) shows the output displacements at different beam lengths, and figure 5(b) shows the output forces at different output displacements for the bent-beam number from 1 to 4. From figure 5(a), the beam length, L, must be 335.23 μm at least to provide 9 μm apex displacement. Here, 400 μm is chosen in bent-beam microactuators. Then, the spring constants of welding units 1 and 2 are

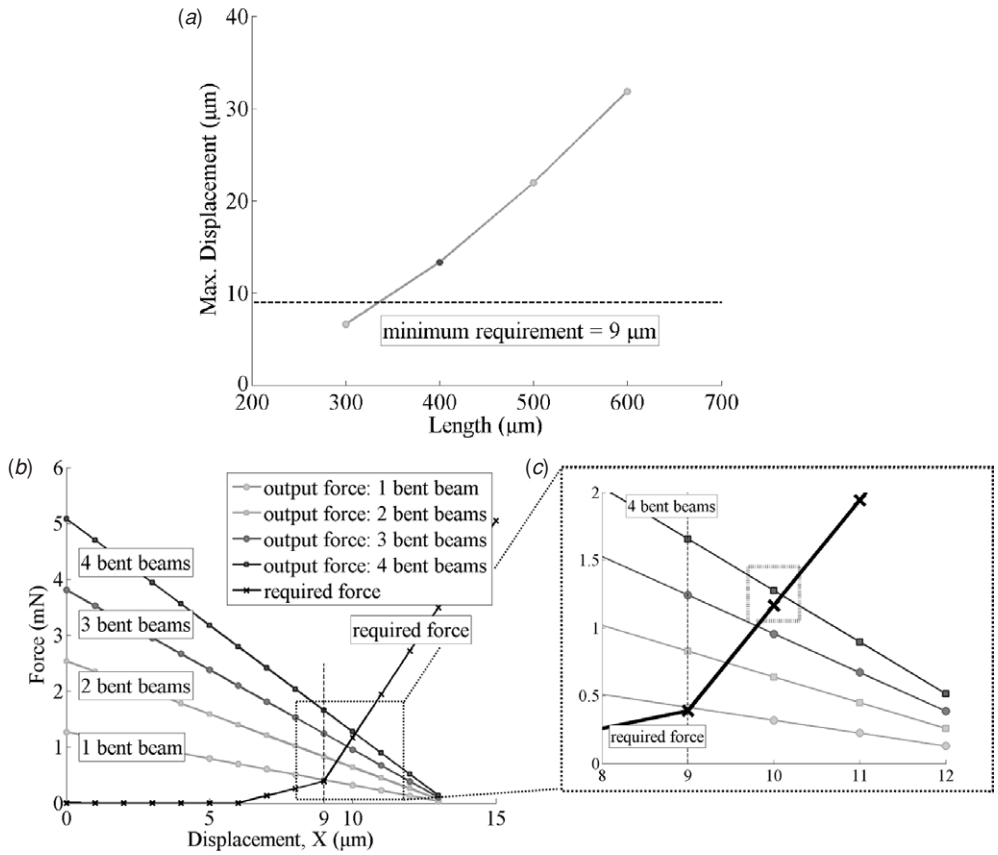

Figure 5. (*a*) Simulated maximum displacements of the apex, d_{max}, under different beam lengths. (*b*) Output forces at different displacements of the apex, *X*, with different numbers of bent beams, as well as the required force at three operation stages. (*c*) The enlargement of the region around the 10 μm apex displacement.

determined to be 129 N m^{-1} and 518 N m^{-1}, respectively. From the dimensions specified in figure 4, the operation of the actuation unit can be divided into three stages, based on the apex displacement, *X*, as follows:

(1) 0 μm $< X <$ 6 μm: the actuation unit moves freely.
(2) 6 μm $\leqslant X <$ 9 μm: the actuation unit pushes only welding unit 1.
(3) 9 μm $\leqslant$ X: the actuation unit pushes both welding units 1 and 2.

In figure 5(*b*), the required forces at the above three stages are also plotted, where slope changes at the displacements of 6 μm and 9 μm due to different effective mechanical spring constants at three stages. From figure 5(*b*), an actuation unit with at least four bent beams in parallel can provide sufficient actuation (1.27 mN) to overcome the mechanical force (1.16 mN) at the displacement of 10 μm. Here, eight bent beams in the actuation unit are fabricated to further ensure sufficient force.

4. Fabrication

The fabrication process is illustrated in figure 6. Figure 6(*a*) shows the viewing direction and location of the cross-section AA′ along welding unit 2. First, oxide thin film is grown as an electrical isolation layer (figure 6(*b*)), and then the FH-6400 photoresist is coated and patterned to act as the sacrificial layer. The Cu/Ti thin film of 120/20 nm is then deposited as the adhesion and seed layer, respectively (figure 6(*c*)). Another 15 μm thick AZP-4620 photoresist is coated and patterned. Then, 10 μm thick nickel is electroplated to form the metal structure (figure 6(*d*)). The temperature of the electroplating process is 50 °C, and the current density is 20 mA cm^{-2}. After removing the electroplating mold and the seed layer underneath the electroplated Ni structure, the device is then released by stripping the sacrificial layer FH6400 with acetone (ACE) (figure 6(*e*)). A picture of one fabricated structure before assembly is shown in figure 7, and the dimension variation between design and fabrication is within 2 μm. By following the welding procedure illustrated in figure 2, welding units 1 and 2 could be fused together in a successful micro resistance welding trial.

5. Measurements

In order to investigate the performance of the proposed micro resistance welding technique, measurements on electrical and mechanical properties are performed.

5.1. Electrical and mechanical properties

In this study, welding current, contact resistance and welding time are recorded during the resistance welding tests.

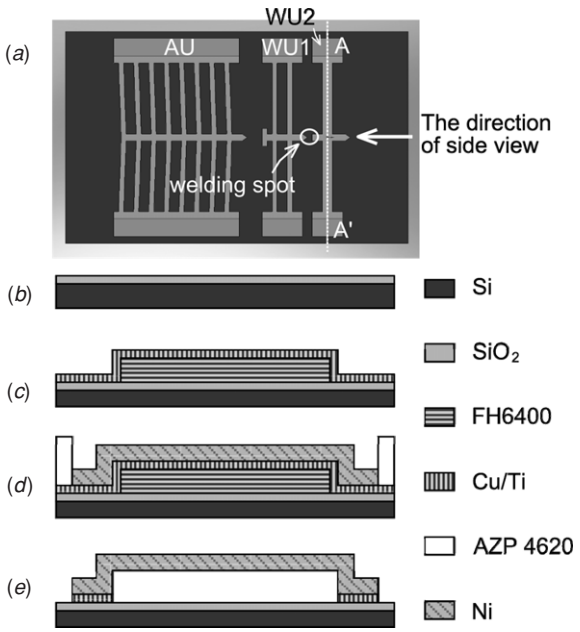

Figure 6. Fabrication process flow of the micro welding structure (side view of AA′ cross section): (*a*) The top view of the microstructure labeled with line AA′, (b) silicon oxide growth, (*c*) photolithography with the FH6400 photoresist and Cu/Ti thin film deposition, (*d*) nickel electroplating and (*e*) release structure.

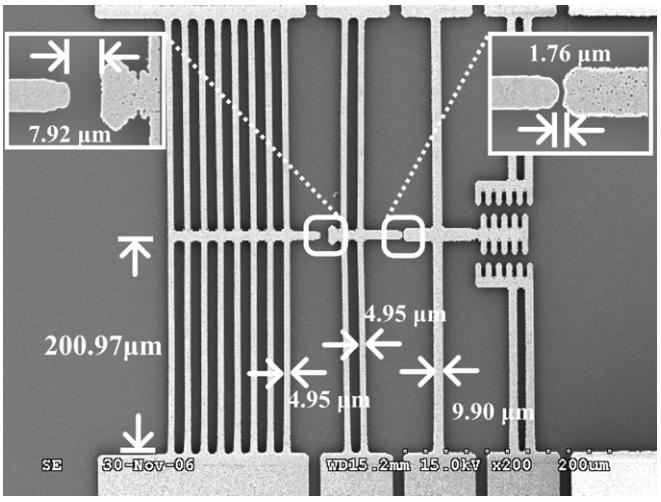

Figure 7. The SEM pictures of the fabricated micro welding structure before welding.

Furthermore, contact pressure having a direct influence on the initial contact resistance which is defined as the contact resistance at the welding site before welding is also recorded. In contrast to initial contact resistance, post-contact resistance is defined as the resistance at the welded site after welding. The initial contact resistance reflects the surface conditions at the contact interface before welding, and the post-contact resistance characterizes the quality of the welding results after welding. It is difficult to measure initial or post-contact resistance directly. Our resistance measurement is performed by measuring the resistance between two pads; therefore, the total resistance along the path will include not only the contact resistance, but also the resistance from the rest of the nickel structure. The resistance due to the nickel structure before contact is measured first, and then is subtracted from the measured total resistance to determine the contact resistance.

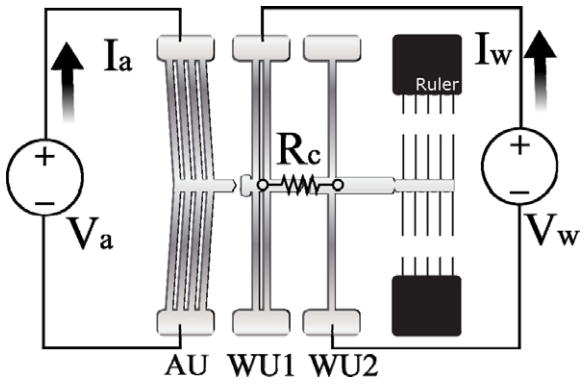

Figure 8. Schematic diagram of measuring electrical characteristics.

The schematic diagram to measure the electrical characteristics of the welding voltages and currents (V_w, I_w) as well as driving voltage and current (V_d, I_d) for the thermal microactuator is shown in figure 8; then the structural resistance and contact resistance, R_c, at the welding site, can be calibrated.

The measurement of the welding strength is also performed using a probe tip to pull the welded joint. By measuring the beam deflection of welding unit 2, the bonding force and the welding strength can be calculated from the spring constant and the deflection just before separation.

5.2. Experimental setup

The dc welding voltage is controlled through a programmable power supply with a resolution of 0.01 V. In order to avoid thermal shock, the welding voltage is set from zero and gradually increased to the maximum value about 0.9 V with a slope of +30 mV s^{-1} (the heating stage). After keeping the maximum voltage for few seconds (the welding stage), the applied power is then gradually turned off with a slope of −30 mV s^{-1} (the cooling stage).

During the welding process, the values of applied voltage and current are retrieved at 6 Hz. Also, the images from optical microscopy during the welding process are detected by a CCD camera. After applying power to the actuation unit, welding unit 1 is pressed to contact with unit 2. Then, the initial contact resistance is calibrated before applying welding current. After the welding process, the resistance of the welding site, so-called post-contact resistance, is also calibrated.

6. Results and discussions

The electrical and mechanical properties, such as welding energy, contact resistance and welding strength, are reported here. The relation between these parameters and the effects are also discussed.

In the tests, the driving voltage to the actuator unit and the welding voltage to the welding structure are two major controlled parameters. In order for the actuator unit

to provide enough displacement, different driving voltages ranging from 0.6 V to 1.3 V are applied to the actuator for it to push welding unit 1 to contact with welding unit 2 to have different contact pressures, and the corresponding initial contact resistance can be calibrated. Then, the welding test proceeds by applying voltage to the welding structure to have joule heating at the welding site, and the corresponding current, I_w, is automatically recorded by the power supply. In section 5.2, it states how the welding voltage is controlled during the welding process. The welding voltage is set to zero and gradually increased with a slope of +30 mV s^{-1} (the heating stage) for a certain time, ranging from 26 s to 32 s. Then keeping that voltage for 1 s (the welding stage), the applied power is gradually turned off with a slope of -30 mV s^{-1} (the cooling stage). By organizing these recorded data, including welding voltage, welding current and welding time, the welding energy can be calculated by $Q = \int (VI)\, dt$ numerically. For the successfully welded test samples, the post-contact resistance and the welding strength can be measured.

An example of the successful micro resistance welding process is given in figure 9. Figure 9(*a*) is the initial state of micro structures. In figure 9(*b*), the actuation unit pushes welding unit 1 to contact with unit 2. After applying the proper welding energy, the material around the contact point is melted to achieve assembly. Then the microactuator is released, as shown in figure 9(*c*), to complete the micro resistance welding process.

Contact pressure will affect the initial contact resistance directly. The measured results shown in figure 10 indicate that the initial contact resistance decreases with increasing contact pressure evidently, which could be resulted from a larger contact area with larger contact force.

Post-contact resistance represents the resistance at the welded joints after welding. The calibrated data of post-contact resistances at different initial contact resistances from 2.7 Ω to 74.3 Ω are shown in figure 11. It is found that after the welding process, the post-contact resistances of successful cases all gather between 0.1 and 1.15 Ω. The varied range of post-contact resistance is obviously smaller than the range of initial contact resistance. It seems that the conductivity at welded joints becomes more stable regardless of initial conditions.

The amount of welding energy is found to affect the yield of micro resistance welding significantly. As shown in figure 12, when the input welding energy is below the threshold limit, 0.05 J in our cases, the welding trials all fail. For the input energy between 0.05 J and 1 J, there is a transition region from 33.3% yield to 58.3% yield. At high welding energy between 1 and 10 J, the yield can reach 100%.

After the welding process, the successfully assembled structures are examined to determine the welding strength. It is found that the strength increases with decreasing contact resistance, as shown in figure 13. In successful trials, the maximum welding strength can reach 3.09 MPa (74.4 μN) at an initial contact resistance of 2.7 Ω, and the minimum is about 0.13 MPa (3.2 μN) at an initial contact resistance of 57.4 Ω.

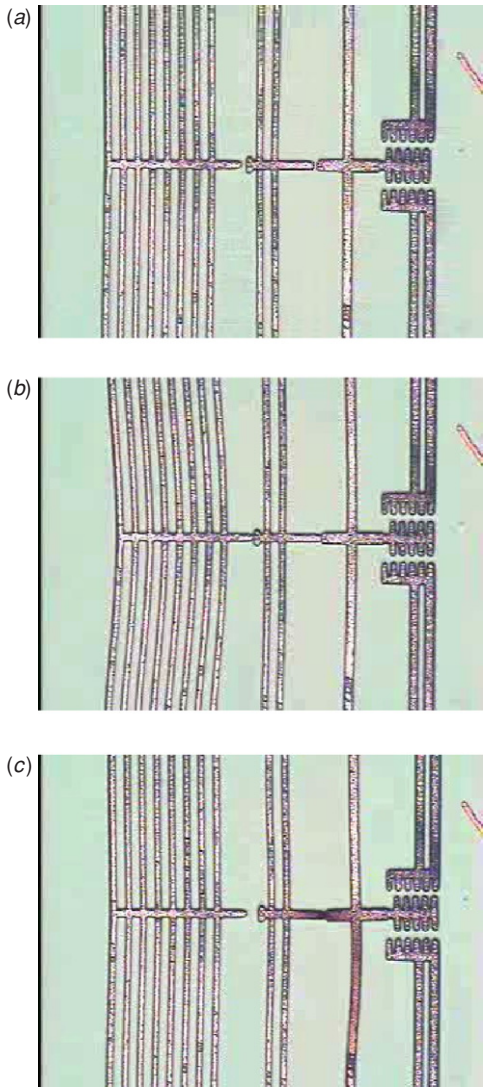

Figure 9. The micro resistance welding process. (*a*) Initial state. (*b*) Actuation unit pushes welding unit 1 to contact with unit 2. (*c*) The pressing force is removed and welding units 1 and 2 are successfully welded together.

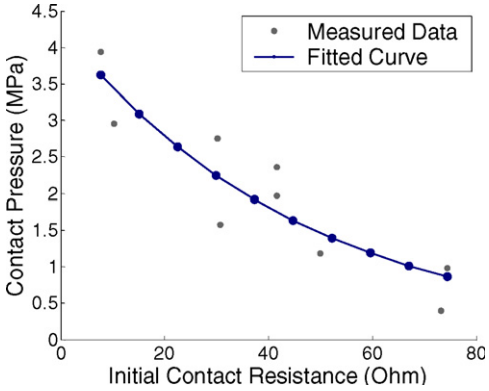

Figure 10. Contact resistance at different contact pressures before welding.

The initial contact resistance shown in figure 12 ranges from 2.7 Ω to 109 Ω. From figure 12, it can be seen that

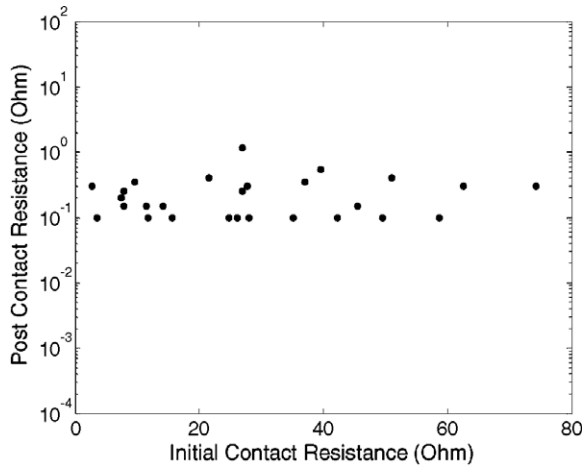

Figure 11. Post-contact resistance at different initial contact resistances.

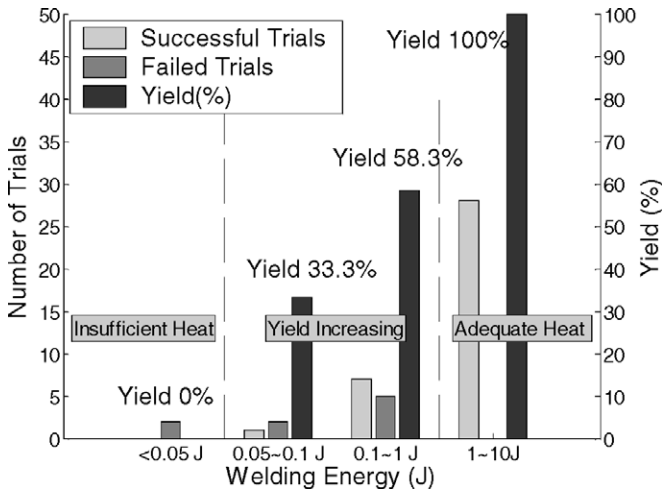

Figure 12. The yield of the welding process under different input energies.

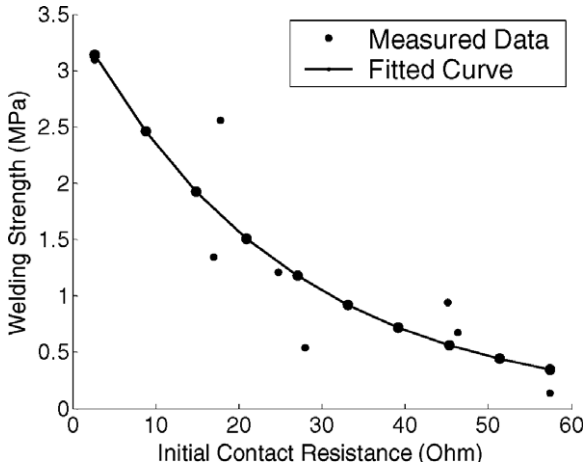

Figure 13. Welding strength with different initial contact resistances.

the welding energy dominates the yield. From equations (1) and (2), at the same voltage and welding time, welding energy increases with increasing current, but decreases with increasing resistance. Therefore, low resistance with a large current is preferred, which is also good for welding strength (figure 13). From figures 10 and 13, it can be found that higher contact pressure induces lower initial contact resistance, and then more energy can be applied to the welding process to generate larger amount of heat, which leads to more melting material to provide better strength. For efficiency, short welding time is desired for fast production, and then a larger current would also be helpful in reducing welding time to meet the required welding energy.

7. Conclusions

Micro assembly by resistance welding with a microactuator is successfully demonstrated and characterized here. It is found that applied welding energy is one of the key factors. When the applied energy is above a certain threshold value, 100% yield can be achieved in our cases. Also, higher contact pressure is shown to provide lower initial contact resistance and better welding strength with shorter welding time. The technique of thermal assembly proposed here could provide good electrical connection and mechanical strength, which would be helpful not only in assembly automation, but also in allowing electrical signal transmission between micro structures through welded joints.

Acknowledgments

This work was supported by the National Science Council (Taiwan) under grant NSC 95-2221-E009-012-MY2. The authors also would like to express appreciations to the Nano Facility Center of National Chiao Tung University for providing facilities and technical support. This work was presented in part at the 2007 IEEE International Conference on Nano/Micro Engineered and Molecular Systems and the 2008 SPIE Symposium on MOEMS-MEMS.

References

[1] Harendt C, Graf H-G, Höfflinger B and Penteker E 1992 Silicon fusion bonding and its characterization *J. Micromech. Microeng* **2** 113–6

[2] Harendt C, Appel W, Graf H-G, Höfflinger B and Penteker E 1991 Wafer fusion bonding and its application to silicon-on-insulator fabrication *J. Micromech. Microeng.* **1** 145–51

[3] Yang H A, Lin C W and Fang W 2006 Wafer level self-assembly of microstructures using global magnetic lifting and localized induction welding *J. Micromech. Microeng.* **16** 27–32

[4] Cheng Y-T, Lin L and Najafi K 2001 A hermetic glass-silicon package formed using localized aluminum/silicon-glass bonding *J. Microelectromech. Syst.* **10** 392–9

[5] Harsh K F, Bright V M and Lee Y C 1999 Solder self-assembly for three-dimensional microelectromechanical *Systems Sensors Actuators* A **77** 237–44

[6] Syms R R A 1998 Rotational self-assembly of complex microstructures by the surface tension of glass *Sensors Actuators* A **65** 238–43
[7] Syms R R A 1999 Surface tension powered self-assembly of 3-D micro-optomechanical structures *J. Microelectromech. Syst.* **8** 448–55
[8] Fedder G K and Howe R T 1991 Thermal assembly of polysilicon microstructures *Proc. IEEE Microelectromech Systems (Nara, Japan)* 63–8
[9] Yeh C-C, Chun J, Chang C-W and Hsu W 2007 Micro assembly by micro resistance welding with electro-thermal actuators *Proc. 2nd Int. Conf. on IEEE Nano/Micro Engineered and Molecular Systems (Bangkok, Thailand)* 333–6
[10] Chang C-W and Hsu W 2008 Characterization of microresistance welding with electrothermal actuator for microassembly *Proc. SPIE* **6884** 68840G
[11] Wilcox W L *et al* 1980 *Welding Handbook: Resistance and Solid-State Welding and Other Joining Process* vol 3 ed W H Kearns (Miami, FL: American Welding Society) pp 2–3
[12] Sinclair M J 2000 A high force low area MEMS thermal actuator *Proc. 7th Intersociety Conf. on Thermal Phenomena (Las Vegas, NV)* vol 1 pp 127–32
[13] Que L, Park J-S and Gianchandani Y B 2001 Bent-beam electrothermal actuators: Part I. Single beam and cascaded devices *J. Microelectromech. Syst.* **10** 247–54